J Mar Sci Technol (2010) 15:230–241
DOI 10.1007/s00773-010-0088-8

ORIGINAL ARTICLE

Hydro- and aerodynamic analysis for the design of a sailing yacht

Wu-Joan Kim · Jaehoon Yoo · Zhengshou Chen · Shin Hyung Rhee · Hye-Ryoun Chi · Haeseong Ahn

Received: 8 March 2009 / Accepted: 14 March 2010 / Published online: 17 April 2010

Abstract The results of the design analysis for a sailing yacht's hull and sails are reported. The results were used to confirm the design of a 30 ft long sloop, which was planned, designed, and built in Korea for the first time in history. Flows around a sailing yacht above and under the free surface were analyzed separately using both computational and experimental methods. For the underwater flow analysis, turbulent flow simulations with and without free surface wave effects were carried out for the canoe hull with keel/rudder. The computed drag and side forces on the hull model were compared with the measurement data obtained from the towing tank experiments. In order to assess the sail performance, another set of computations was carried out for the flow around a sail system composed of main and jib sails with a mast. The present study demonstrates that, for the design analysis of a sailing yacht, computational fluid dynamics techniques can be utilized with a reasonable level of confidence.

W.-J. Kim · J. Yoo · Z. Chen
Department of Ocean Engineering, Mokpo National University, Jeonnam, Korea

S. H. Rhee (✉)
Department of Naval Architecture and Ocean Engineering, Research Institute of Marine Systems Engineering, Seoul National University, Seoul, Korea
e-mail: shr@snu.ac.kr

H.-R. Chi
Daewoo Shipbuilding and Marine Engineering Co., Ltd, Gyeongnam, Korea

H. Ahn
Maritime and Ocean Engineering Research Institute, Korea Ocean Research and Development Institute, Daejeon, Korea

Keywords Sailing yacht · CFD · Design analysis

1 Introduction

Sailing yacht design is generally based upon empirical formulas and the designer's experience, with the occasional use of model tests, such as towing tank experiments for the hull form and wind tunnel experiments for the sail design [1]. However, it is quite expensive to obtain useful hydro/aerodynamic information from the model tests, because there are so many factors to be considered when attempting to predict the sailing yacht's performance, such as the wind direction, advancing angle, interference between sails, heel and yaw angles, and the flow interaction between keel and rudder. Therefore, in addition to model tests, computational fluid dynamics (CFD) is being widely adopted as an efficient tool for assessing ship performance, and is used extensively for the hydro/aerodynamic design analysis of sails, hull form, and appendages. There have been many reports on the use of CFD for sailing yacht design, including its application to state-of-the-art International America's Cup Class (IACC) yachts [2, 3] and the boat motion on the free surface [4]. In order to support CFD simulations, selective towing tank experiments are also carried out to validate the CFD results. Although CFD is now a popular tool for sailing yacht design, physical model tests are still the most crucial part of the design process [5].

Flow analysis for a sailing yacht is much more complicated than that for a commercial ship, largely because of their different propulsion mechanisms. Sails can be considered a system of zero-thickness foils with an attack angle, and so they generate side forces as well as thrust. The so-called lateral resistance on the underwater portion of the hull and the keel/rudder should balance the side forces produced by

the sails; otherwise the hull will drift. Therefore, a sailing yacht almost always advances with a leeway angle, i.e., the heading angle of the yacht centerline with respect to the advance direction. Sailing with this leeway angle results in an attack angle that leads to the production of side forces by the keel/rudder. Side forces from the sails and the keel/rudder also produce a coupling moment that acts as the heeling moment. The hull will then heel until this heeling moment is balanced by the righting moment due to buoyancy.

A 30 ft long sloop was designed and built by the Maritime and Ocean Engineering Research Institute (MOERI). The present study is concerned with the hydro- and aerodynamic design analysis of the yacht, which was performed to confirm the newly developed design. In other words, the hull and sail design was analyzed and it was confirmed that the performance satisfies the desired velocity made good (VMG) results. Towing tank experiments were carried out in the MOERI towing tank to measure the hydrodynamic forces acting on the hull. Drag and side forces were measured in heeling and yawing conditions. Turbulent flow simulations around the hull and the sails were carried out separately using a CFD code that solves the Reynolds-averaged Navier–Stokes (RANS) equations. For the underwater flow simulations, the canoe hull with the keel/rudder was considered with and without free-surface wave effects. For the airflow simulations, both main and jib sails were considered with the mast. The computational results were compared with the data from the towing tank experiments and the existing wind tunnel test data [6].

Better agreement with the towing tank experimental data is obtained when the free-surface wave effects are included. It was also confirmed that the heel angle has a large influence on the hydrodynamic performance of a yacht hull. The flow field around the main sail significantly depends on the jib sail angle, since the main sail is placed in the wake of the jib sail. The calculated center of effort (i.e., the pressure center of the sail system) is much different from the geometrical center of the sail surface, although this is commonly employed as an empirical center of effort.

The present paper is organized as follows. The geometry of the designed hull and sails is presented next. Then the experimental and computational methods are described, followed by the flow analysis results for the underwater and air flows around the hull and sails, respectively. We then make some concluding remarks.

2 Designed hull and sails

2.1 Hull

The 30 ft long sloop, named KORDY30, was designed using traditional ship design methods for commercial ships along with empirical formulas for sailing yachts [7]. Since it was the first sailing yacht designed in Korea, various requirements were imposed: an affordable yet multipurpose sailing yacht that incorporates state-of-the-art technology was required. The new design's parent ship was the "Mini 6.5," introduced at the Madrid Diseno De Yates '04, which is smaller than the KORDY30's required size. For the desired size range, three reference ships were selected: "Columbia 30," "Auklet 9," and "Yamaha 31 S." Details for the parent ship and the reference ships are available in Yoo et al. [7], as well as on the internet. The new design has a round-bottomed canoe hull with a long keel and a rudder. Figure 1 shows an artist's rendering of the complete KORDY30. The principal particulars are given in Table 1. For the towing tank experiments, a model hull with a scale ratio (λ) of 1/3 was manufactured. All of the measurements and simulated flows around the yacht's hull were conducted on the model scale.

2.2 Main and jib sails

The KORDY30 was equipped with a sloop sail system consisting of a main sail and a jib sail, as shown in Fig. 2. The sections of the main and jib sails were shaped as the NACA $a = 0.8$ mean camber line without thickness. Note that this shape is quite close to that of modern cloth sails. The luffs (i.e., the leading edges) of both the main and jib sails were fixed; however, because of the wind load, the leeches (i.e., the trailing edges) had to be adjusted, except

Fig. 1 Artist's rendering of KORDY30

Table 1 Principal particulars of the KORDY30

	Value	Definition
LOA (m)	9.142	Length overall
L_{WL} (m)	8.245	Waterline length
B (m)	3.024	Beam (max.)
Tc (m)	0.400	Draft w/o keel
T (m)	1.900	Draft with keel
∇ (m^3)	3.298	Displacement
Wetted surface area (m^2)	15.60	Hull
	2.84	Keel
	1.18	Rudder

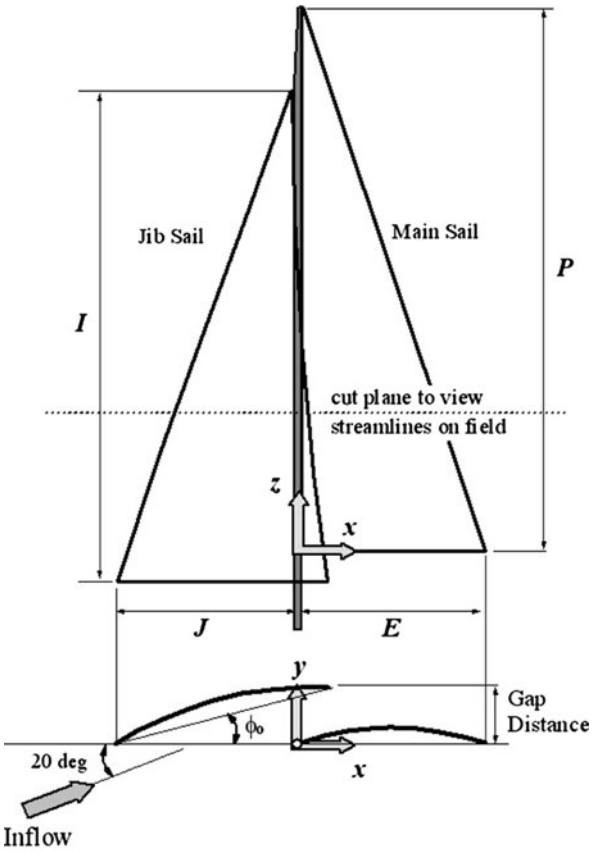

Fig. 2 Sloop sail system

at the foot end of the main sail, as shown in Fig. 3. Figure 3 shows the typical sail shape under close-hauled conditions. The baseline angle of the main sail was varied as 0°, 5°, 10°, 15°, and 20° at 0, 25, 50, 70, and 100% of the height, respectively. The camber of the main sail at each height is given in Table 2.

The geometrical parameters and shape of the jib sail under close-hauled conditions are given in Table 3 and

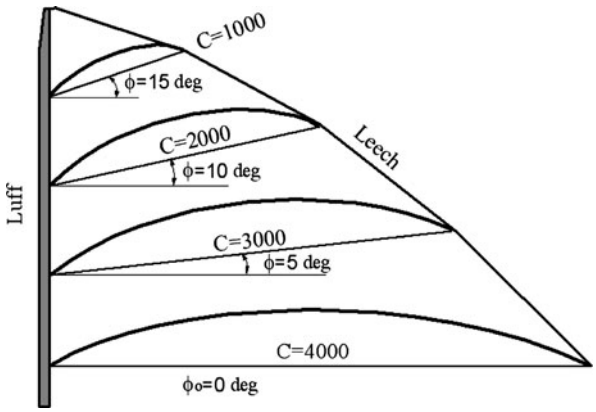

Fig. 3 Geometry of the main sail

Table 2 Geometrical parameters of the main sail

Location	Foot	25%	50%	75%	Top
Height (mm)	0	3000	6000	9000	11900
Chord length (mm)	4000	3000	2000	1000	10
Angle (°)	0	5	10	15	20
Camber ratio	8	10	12	14	16

$P = 11.9$ m, $E = 4.0$ m, area of main sail $A_M = 24.0$ m^2

Table 3 Geometrical parameters of the jib sail

Location	Foot	25%	50%	75%	Top
Height (mm)	0	2750	5500	8250	11000
Chord length (mm)	C_1	75% C_1	50% C_1	25% C_1	10
Angle (°)	Φ_0	1.25 Φ_0	1.5 Φ_0	1.75 Φ_0	2.0 Φ_0
Camber ratio	8	10	12	14	16

$C_1 = C_0 \times (1 +$ overlap length) (mm), C_0: length of jib sail foot 3900 mm, Φ_0: baseline angle of jib sail foot (jib angle)

Fig. 4. The jib sail's leech overlapped with the main sail's luff near the foot, and this overlap length is an important parameter that determines the interference between the two sails. The baseline angle of the jib sail, called the jib angle, was also a key parameter, since it determines the relative angle of the wind into the jib sail and the inflow (i.e., the wake of the jib sail) into the main sail.

3 Experimental method

3.1 Towing tank tests

The experiments were carried out in the towing tank of the Korea Ocean Research and Development Institute. The tank dimensions were 200 m (long) × 16 m (wide) × 7 m

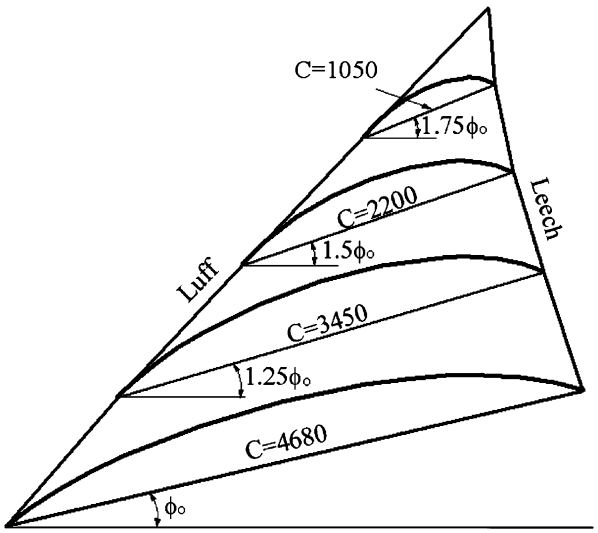

Fig. 4 Geometry of the jib sail

Fig. 5 Towing system

(deep), and the maximum towing speed was 6 m/s. The model scale ratio for the towing model was set to 1/3, considering the towing speed and the load cell capacity. The model was manufactured from wood, with the rudder and keel attached. The keel was manufactured to be removable, thus allowing investigations of the hydrodynamic performances of the canoe hull with and without the keel. A special clamping device (Fig. 5) was prepared that is able to rotate with the load cell and fix the model hull with heel and yaw. The load cell was attached at the location of the mast.

While the model hull was towed at the predefined fixed attitude, the longitudinal (Fx) and transverse (Fy) forces were measured and converted to drag and side forces, as shown in Fig. 6. When the model was forced to heel, in order to investigate the hydrodynamic performance under heeling conditions, the displacement changed. Under

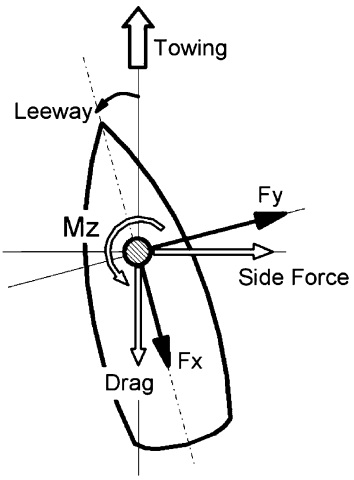

Fig. 6 Directions of the forces exerted on the yacht hull

heeling conditions, therefore, the draft was first adjusted in order to make the displacement the same as that when the model was not heeling, and then the force measurements were made. Further details of the towing tank tests are reported in Yoo and Ahn [8].

When a sailing yacht advances in the wind, it heels and yaws, and the direction of the sails strongly depends on the wind direction. As such, the hull attitude and the wind conditions should be defined at each speed. In the present study, the Designer Version 2004 of the Offshore Racing Congress (ORC) Velocity Prediction Program (VPP) was used to obtain the design conditions, and the towing conditions were determined, with the optimum point upwind considered to be the maximum VMG, and that downwind considered to be the minimum VMG. The optimum running attitude was also obtained based on the VPP results.

The model ship was towed with Froude's corresponding speed; i.e., the ratio of the speed of the full-scale ship to that of the model hull was the square root of the model scale ratio ($\lambda^{1/2}$). The design speed of the full-scale yacht was 3.34 m/s (= 6.5 knots), and so the speed of the model hull was set to 1.93 m/s. The corresponding Reynolds number (Re) based on the model hull length was 5.86 million, and the Froude number (Fr) was 0.372. The design leeway and heel angles used in the tests were 3° and 20°, respectively. The towing tests were conducted with varying heel angles at a leeway angle of 3°, and with varying leeway angles at a heel angle of 20° (see Table 4).

3.2 Wind tunnel tests

The experiments were carried out in the wind tunnel of the Chungnam National University of Korea. The test section dimensions were 5.2 m × 1.8 m × 1.8 m, and the wind speed was set to 45 m/s at maximum. The sail model was

Table 4 Experimental conditions for towing tank tests

	Value	Definition
Model scale	3.0	L_S/L_M
Model length	3.047 m	$(LOA)_M$
Heel variation	With keel/rudder	Vs = 6.5 knots
0°, 10°, 20°, 30°		Leeway = 3°
Leeway variation	With keel/rudder	Vs = 6.5 knots
0°, 1°, 2°, 3°		Heel = 20°

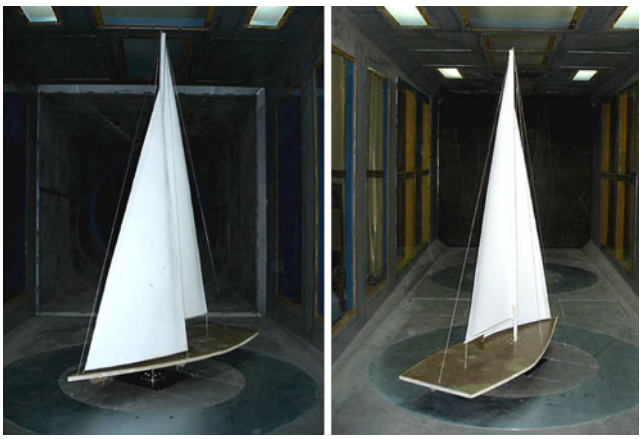

Fig. 7 Wind tunnel experimental setup for sails

made of fiberglass-reinforced plastics (FRP), had a scale ratio of 1/9, and incorporated some rigging, such as a boom, side shrouds, and fore and after stays. Figure 7 shows the equipped model sails in the wind tunnel. A three-component load cell was installed under the sail model with a deck-sized flat plate. The experiments were carried out for a wind speed of 10 m/s. A more detailed description of the experimental study is available in Yoo and Kim [6].

4 Computational methods and conditions

4.1 Grid generation and flow solver

Multiblock structured/unstructured grids were generated using the commercial grid generation package GRIDGEN. The CFD codes employed for the present study were the commercial codes FLUENT 6.2 and CFX 12. Both codes solve the RANS equations with second-order-accurate discretization schemes. For turbulence closure, the standard k–ε model was adopted with a wall function for FLUENT 6.2, while CFX 12 employs the k–ω SST model. Note that FLUENT 6.2 was used for the hydrodynamic analysis, and CFX 12 was used for the aerodynamic analysis.

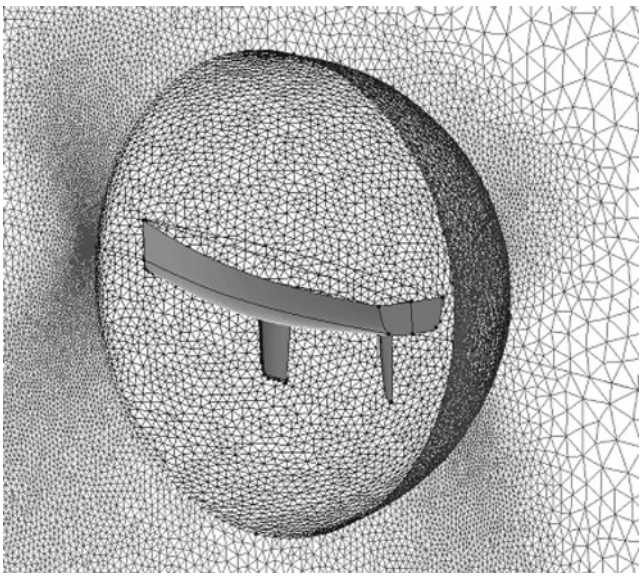

Fig. 8 Unstructured grids around the yacht hull and appendages

Computations were first performed for turbulent flows around the canoe hull and appendages (i.e., keel and rudder). Unstructured grids with as many as 1.1 million cells were used for flows around the hull and appendages with and without free-surface wave effects, as shown in Fig. 8. Next, grids of 1.5 million cells were used for flows around the main and jib sails along with the mast. Figures 9 and 10 show the representative features of the grids. Although it is desirable to simulate the flows around the yacht hull and sails at the same time as the free surface waves, the flows around the hull and sails were analyzed separately in the present study. This is mainly to simplify the analyses and to better focus on the separate information needed for the hull and sail designs.

4.2 Computational conditions

The computational conditions were the same as the experimental conditions. For the flows around the yacht hull, the free surface was first treated as a symmetry plane (i.e., no wave effects were considered). The volume of fluid (VOF) method was then used for the simulations with free-surface wave effects. It should be noted that the near-field free-surface waves were of primary interest here, due partly to the limited scope of the present study and the computer resources available.

In order to meet the constant displacement requirement with heel angles, the grid was rotated first, and then the drafts on the port and starboard sides were adjusted until the calculated displacement reached the initial even-keel condition displacement. Table 5 provides the resulting drafts on the port and starboard sides, and Fig. 11 shows the heeled hull shapes. The abovementioned method of

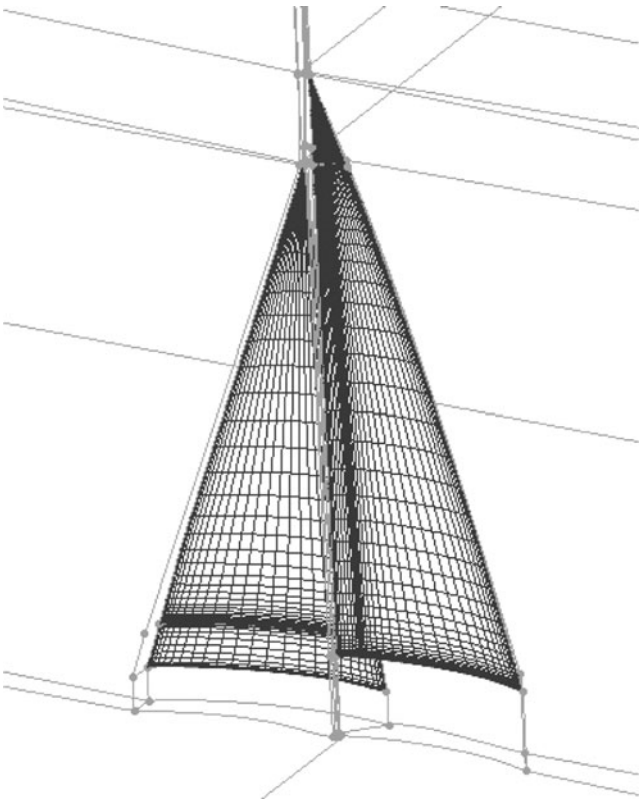

Fig. 9 Surface grids on the main and jib sails with mast

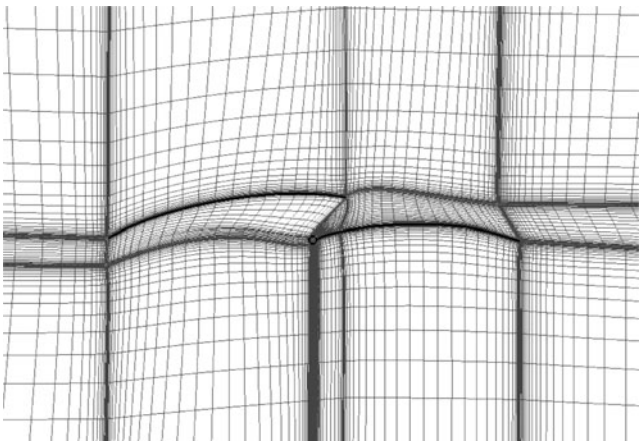

Fig. 10 Field grids around sails (view at a constant height)

determining the drafts under heeling conditions can be used for the hull form design as well.

The sail shape varies when the wind blows because the rig and mast are deformed. The wind direction changes when the yacht is heeled. Furthermore, the viscous boundary layer on the sea surface certainly modifies the inflow velocity profile. However, in the present study, constant air inflow was considered with an attack angle of 20° and a wind speed of 10 m/s. Note that this is based on the previous wind tunnel tests by Yoo and Kim [6].

Table 5 Wetted surface area and drafts at various heel angles (model scale)

Heel	Wetted surface (m^2)	Starboard Ts (cm)	Port Tp (cm)
0°	2.1501	13.000	13.000
10°	2.0911	19.706	6.148
20°	2.0669	26.577	2.094
30°	1.9637	29.126	0.030

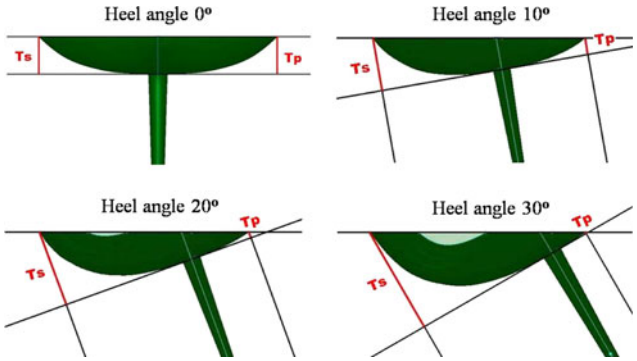

Fig. 11 Hull shapes and drafts at various heel angles

Table 6 Computational conditions for flow simulation around sails

Case	Overlap % of E	Jib angle Φ_0 (°)
1	20	5
2		10
3		15

The deck of the yacht was considered a symmetry plane, and a flat plate was used for it in the wind tunnel tests. This is another reason why the hull and sail were treated separately in the present study. Table 6 summarizes the test conditions for flows around sails. The overlap length between the main and jib sails was set to 20% of the main sail foot length, while the baseline angle of the jib sail foot was changed. The lift and drag of the sails were normalized to the wind speed and the sum of the one-side areas of the main and jib sails.

5 Flows around a yacht hull

As mentioned in the "Introduction," the side forces on the sails balance the lateral resistance on the underwater portion of the canoe hull and the keel/rudder, while the coupling moment generated by these forces above and under the free surface makes the hull heel until it reaches equilibrium through buoyancy. When the hull heels, there is an

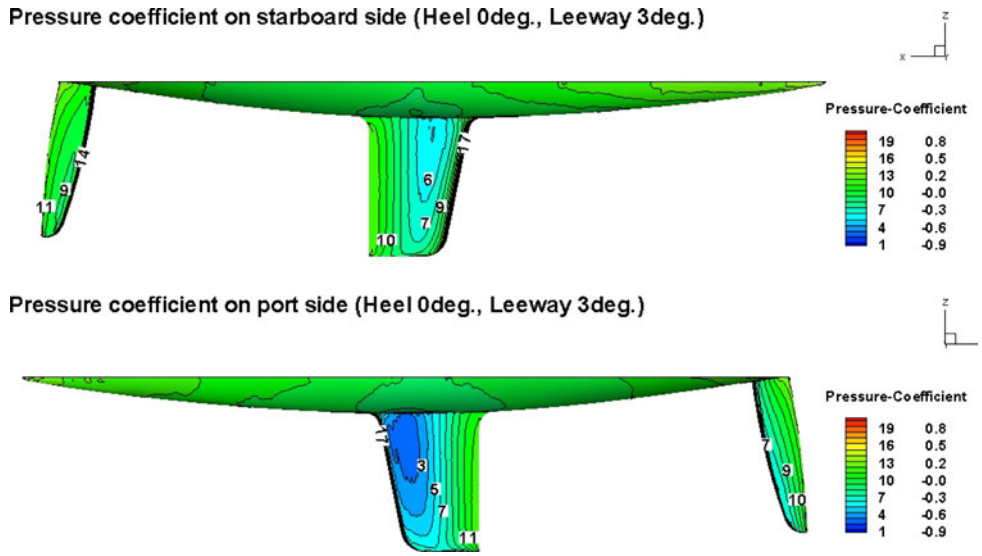

Fig. 12 Pressure contours at a leeway angle of 3° (heel angle 0°)

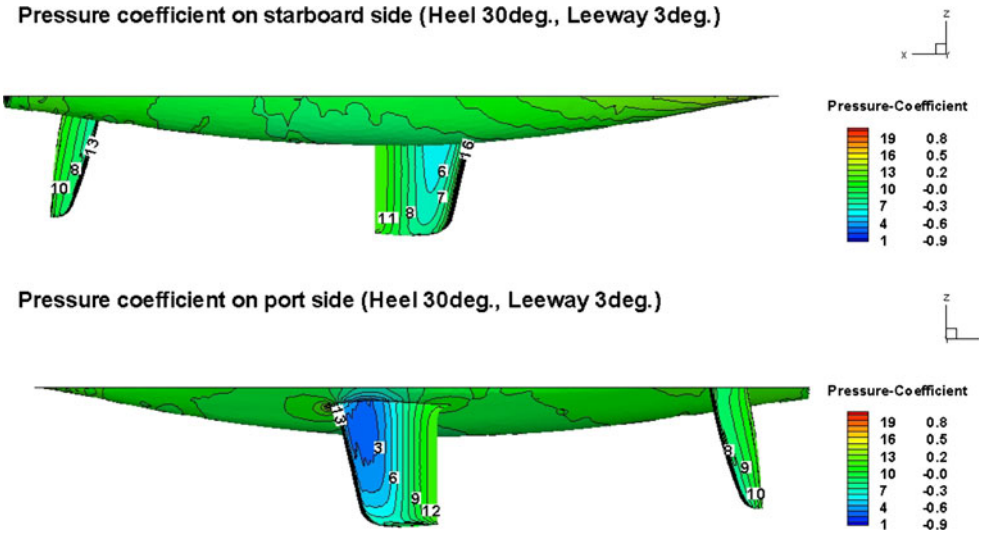

Fig. 13 Pressure contours at a leeway angle of 3° (heel angle 30°)

asymmetry in the flow field [9], and the inflow into the keel differs from that of the symmetric condition without heeling. The flow into the rudder is also influenced by the wake of the keel.

The computed surface pressure contours on the hull surface are shown in Figs. 12 and 13 for a leeway angle of 3° combined with heel angles of 0° and 30°, respectively. When the yacht hull is heeling, the flow field near the hull is also altered, which results in less lateral resistance on the keel/rudder. The rudder area under the free surface is also reduced, resulting in a further decrease in the lifting force produced by the rudder.

As mentioned earlier, a heeled sailing yacht sails with a leeway angle to maintain balance. The yacht examined in the present study was designed to cruise with a heel angle of 20° and a leeway angle of 3°. Changing the leeway angle alters the lift force produced by the keel/rudder, which is confirmed by the surface pressure contours computed for a constant heel angle of 20° with various leeway angles (Figs. 14, 15, 16, 17). The pressure difference between the two sides of the keel/rudder increases with leeway angle, so the lift force by the keel/rudder increases.

Obviously a sailing yacht generates waves when sailing on a real sea. Free-surface wave effects should be included to simulate the flow field correctly. However, it is quite costly to simulate the flow around a yacht including free-surface wave effects (i.e., fine grids and high-performance computing are required). In the present study, as mentioned above, only the near-field free-surface waves were considered. Figure 18 shows a comparison of the waterlines of the rigid free-surface plane condition (dashed lines) and the final equilibrium free-surface condition (solid lines). The

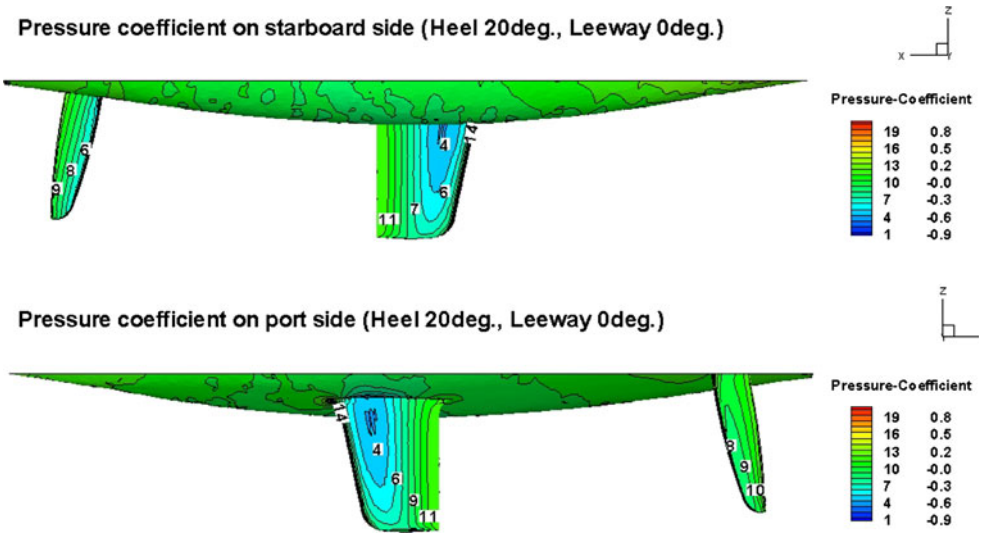

Fig. 14 Pressure contours at a heel angle of 20° (leeway 0°)

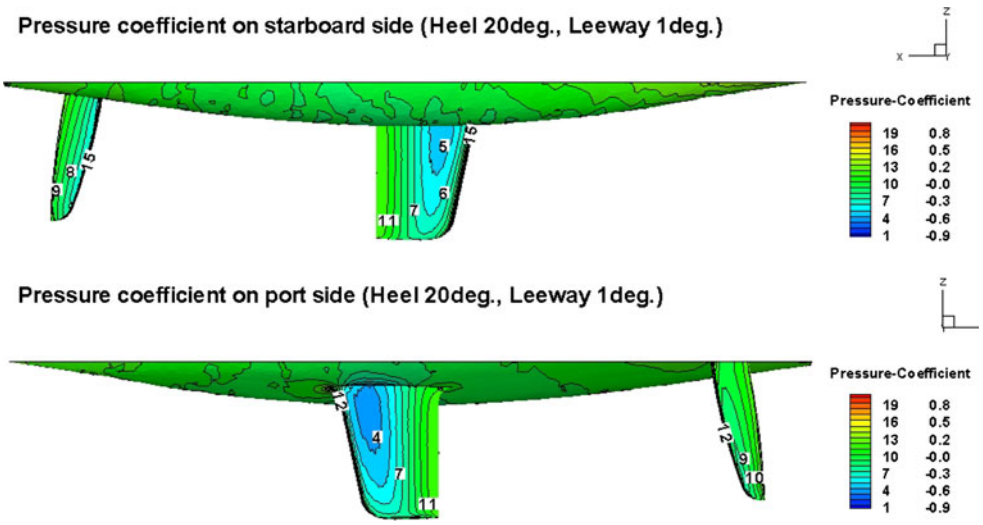

Fig. 15 Pressure contours at a heel angle of 20° (leeway 1°)

dashed lines represent the waterlines used under symmetry plane conditions, which was applied for the simulations performed without free-surface wave effects. On the other hand, the solid lines show the final free-surface shape obtained from the simulations that included free-surface wave effects using the VOF method. Note that, in the present study, the yacht hull was heeled to the starboard side, and the above figures are drawn as seen from the bottom. In the case of a heel angle of 0°, the free surface near the stern region is raised. As the heel angle increases, the waterline is no longer symmetric and changes more dramatically. These waterline changes also alter the flow field around the hull and the submerged shape of the rudder. The resulting drag and side forces when free-surface wave effects are included are different from those for the rigid free-surface plane condition.

The drag and side forces for a leeway angle of 3° with various heel angles are shown in Fig. 19. It was observed experimentally that the drag reaches its minimum at a heel angle of 20°. When free-surface wave effects are not considered, the drag computed for the same heel angle is quite different from the measured drag, while the results obtained when free-surface wave effects are included generally agree with the measured ones. The side forces obtained under rigid free-surface plane conditions also show the opposite tendency to their experimental counterparts, because the elevation of the wave alters the wetted surface and the submerged area of the rudder. It was confirmed that free-surface wave effects play an important role in predicting the correct drag and side force when CFD is applied to evaluate yacht hull performance and balance.

The drag and side forces for the heel angle of 20° with various leeway angles are shown in Fig. 20. Again, when the free surface wave effects are included in the CFD simulations, it is seen that better agreement is obtained with the experimental data, although they are still over-predicted.

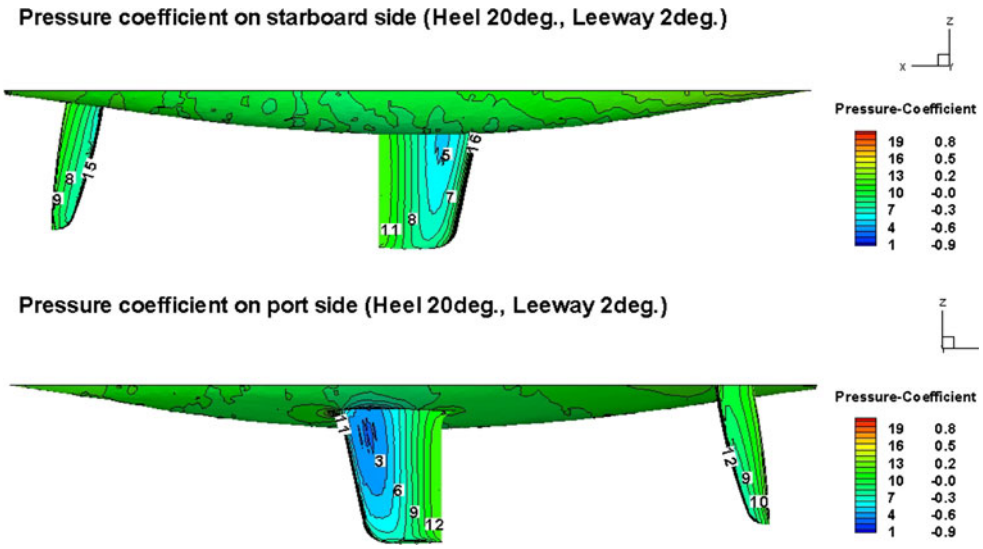

Fig. 16 Pressure contours at a heel angle of 20° (leeway 2°)

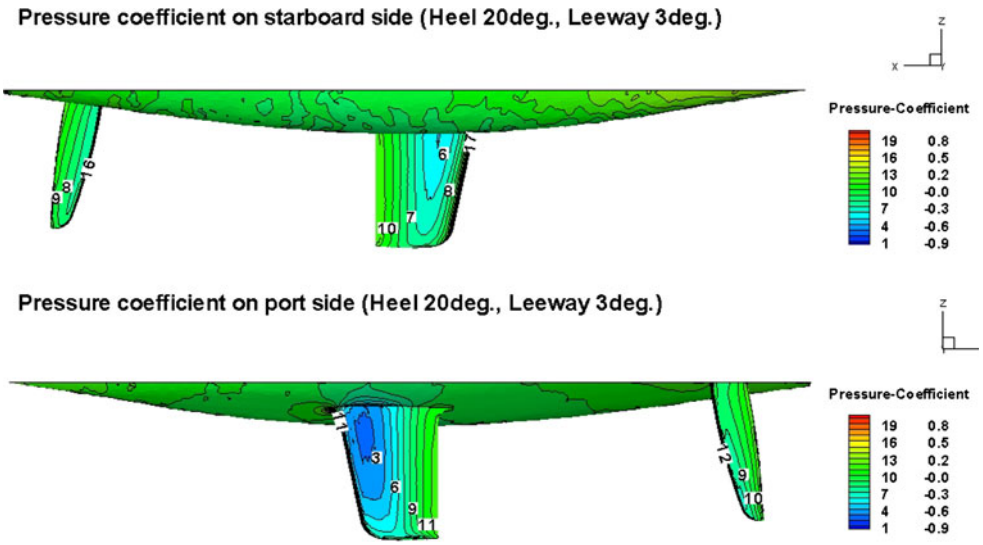

Fig. 17 Pressure contours at a heel angle of 20° (leeway 3°)

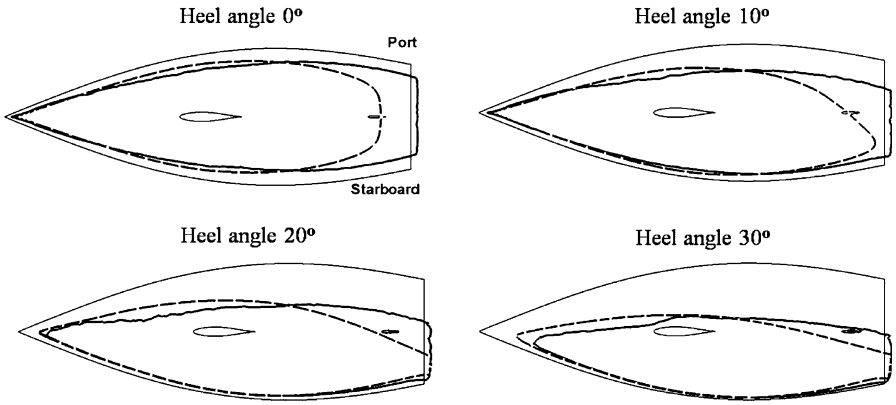

Fig. 18 Waterline shapes at a leeway angle of 3°: *solid lines* for with free-surface wave effects; *dashed lines* for the rigid free surface plane condition)

6 Flows around yacht sails

Turbulent flows around the main and jib sails were simulated, and the results were compared with wind tunnel test data [6]. The pressure distribution on the sail surface is displayed for jib angles of 5°, 10°, and 15° with an overlap length of 20% in Fig. 21. The limiting streamlines on the sail surfaces are also shown in Fig. 22. The wind direction

was 20° with respect to the baseline of the main sail foot. As the jib angle increases, the relative angle of attack for the jib sail decreases. On the windward side, the pressure is higher with a smaller jib angle, since the wind directly hits the jib sail first. However, the main sail shows an opposite tendency, as it is located behind the jib sail (i.e., in the wake of the jib sail). The pressure contours on the leeward side are more dramatic. Flow separation on the jib sail surface is expected at a jib angle of 5°, since the relative angle of attack reaches the stall angle of about 15°, and so the interference between the jib and main sails becomes more complex. Therefore, it is recommended that the lift of the whole sail system (the jib and main sails) should be considered as one (i.e., the total contribution from the two sails).

When the jib angle is 5°, the limiting streamlines on the windward side are straight, while flow separation is observed on the leeward side. On the windward side of the main sail, the flow separated from the jib sail leech attaches and divides. For jib angles of 10° and 15°, the limiting streamlines on the

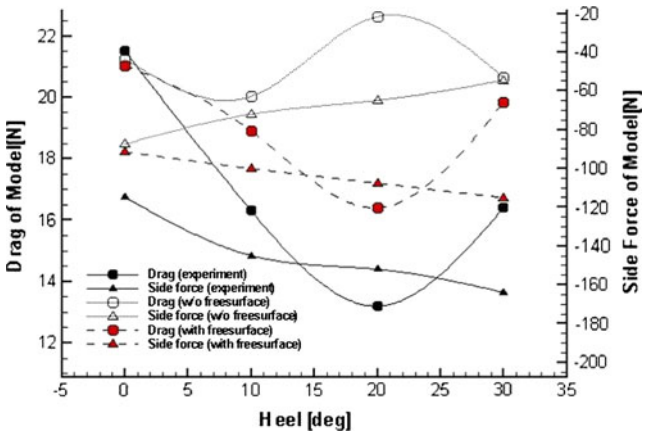

Fig. 19 Drag and side forces with varying heel angles (leeway angle of 3°)

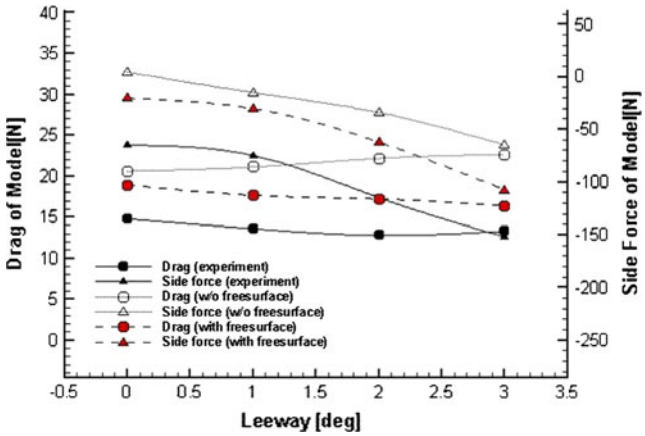

Fig. 20 Drag and side forces with varying leeway angles (heel angle of 20°)

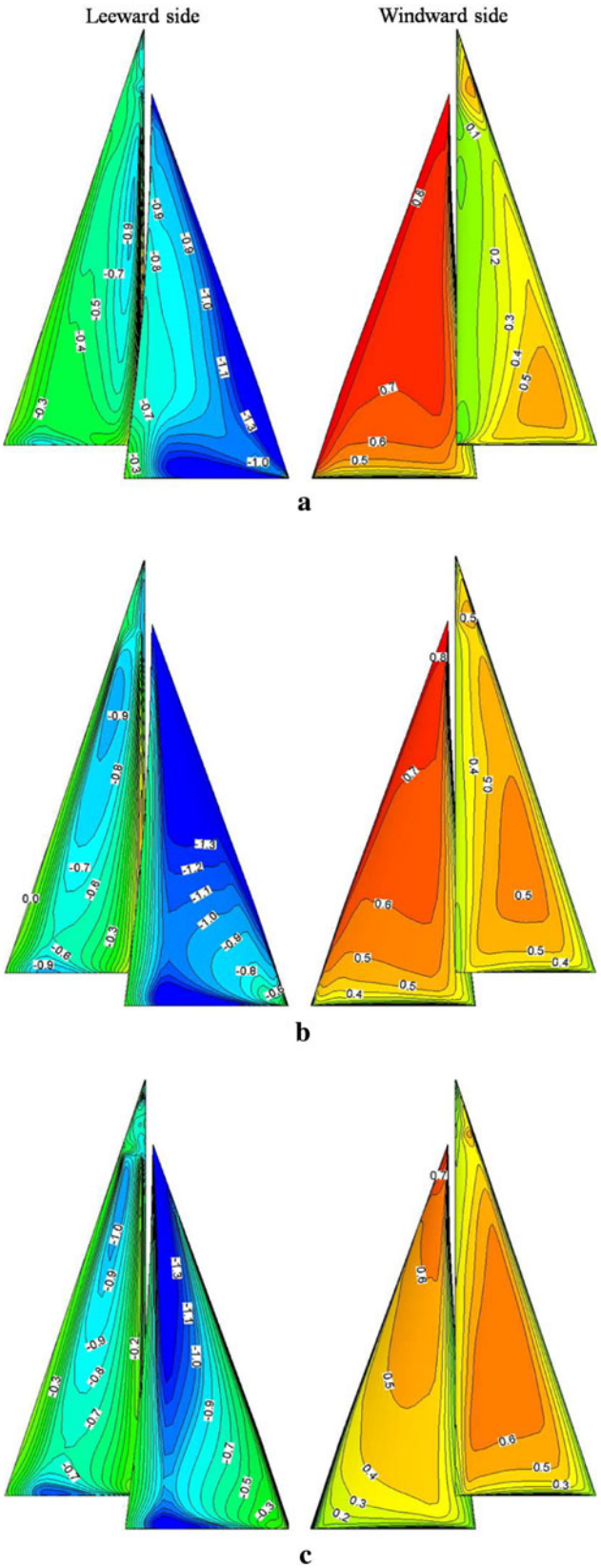

Fig. 21 Pressure contours on the sail surface: *left* (leeward side); *right* (windward side). **a** Jib angle of 5° (case 1), **b** jib angle of 10° (case 2), **c** jib angle of 15° (case 3)

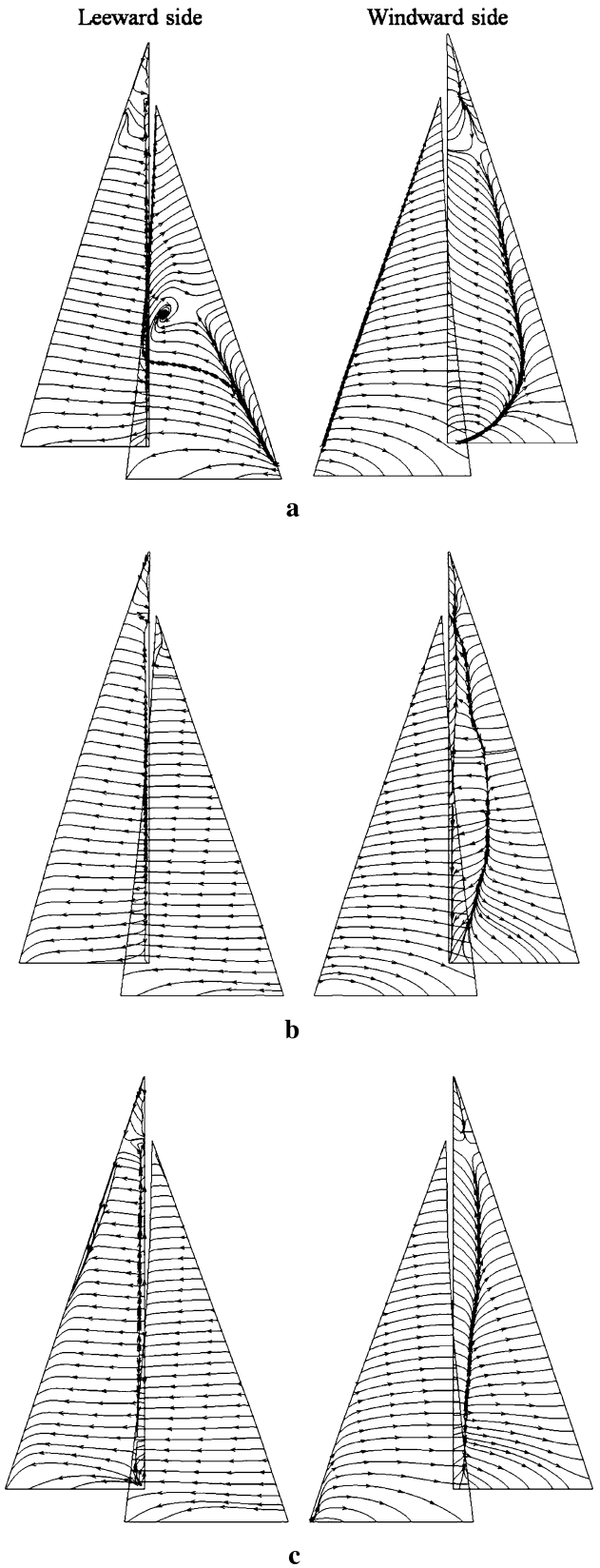

Fig. 22 Limiting streamlines on the sail surface: *left* (leeward side); *right* (windward side). **a** Jib angle of 5° (case 1), **b** jib angle of 10° (case 2), **c** jib angle of 15° (case 3)

leeward side are similar, since the relative angle of attack is reduced, indicating that the existence of the main sail also affects the flow around the jib sail. The distance between the two sails is also an important factor in predicting the sail system performance. It is obvious that the interaction between the jib and the main sails should be considered carefully when evaluating the sail system performance.

The computed drag and lift coefficients were compared with the experimental data [6], as summarized in Table 7. The computed results compare well with the experimental data. When the jib angle is 5°, the jib sail produces more drag than the main sail, while the opposite is true at larger jib angles. This is because the flow separation around the jib sail is severe at a jib angle of 5°, and this separated wake flow has a significant impact on the inflow into the main sail. As the jib angle increases, the flow pattern becomes more streamlined and the drag force decreases. It is observed that the total lift reaches its maximum value when the jib angle is 10°, where the jib sail produces 70% of the total lift. Figure 23 shows the streamlines around the sails in cross-section at 25% of the sails' height from the bottom, which agree with the tendency discussed above.

The pressure center of the sail system, i.e., the center of effort (CE), is generally obtained from simple geometric considerations. Larsson and Eliasson [1] suggested that the geometric center of each sail should be taken as the center of effort, and the CE of the whole sail system should be considered the weighted geometric center of the sails in the system. This approach assumes that the pressure on the sail surface is constant throughout the whole system. In the present study, the CE of the sail system is calculated based on the computed pressure values for the sail system, as presented in Table 8. The calculated CE is indeed considerably different from the one obtained by the empirical formula using simple geometrical considerations, indicating that the CE calculation should be done more carefully, even during early design phases.

7 Concluding remarks

The results of the design analysis for a sailing yacht's hull and sails are reported. The results were used in the design

Table 7 Drag and lift coefficients—CFD results versus experimental data

Jib angle (°)	CFD (present)		Experimental data [6]	
	C_L	C_D	C_L	C_D
5	1.10	0.25	1.39	0.37
10	1.31	0.19	1.43	0.30
15	1.07	0.13	1.40	0.25

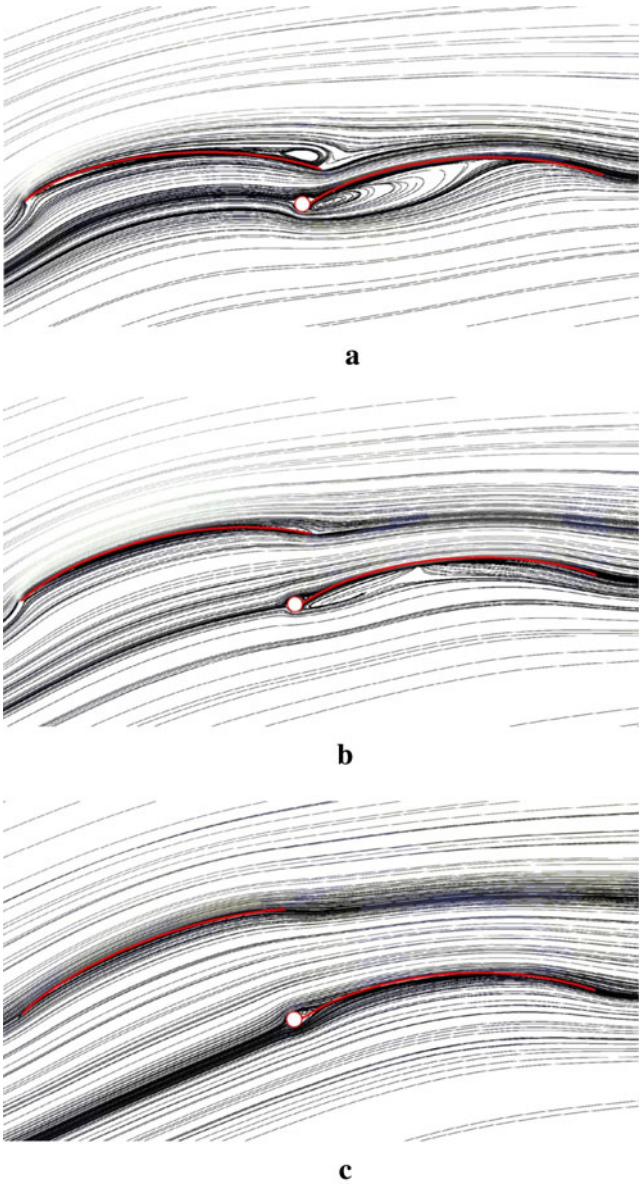

Fig. 23 Streamlines around the sails at 25% of the sails' height from the bottom. **a** Jib angle of 5°, **b** jib angle of 10°, **c** jib angle of 15°

of a 30 ft long sloop, which was planned, designed, and built in Korea for the first time in history. The flows around a sailing yacht hull with keel/rudder and a sail system consisting of the main and jib sails were studied. The forces acting on the yacht hull with various yaw and heel angles were measured in the MOERI towing tank. For the turbulent flow simulations, the RANS equations were solved with the standard k–ε model for turbulence closure. The VOF method was employed in the CFD code in order to include free-surface wave effects. The computed results for the hull with appendages were compared with experimental data. The overall agreement is fairly commendable, but the results computed without the free surface wave effects show a significant deficiency in predicting the drag under the design conditions.

Table 8 Location of the center of effort (CE) at a jib angle of 10°

Location of CE	Present	Empirical formula [1]
Longitudinal	−321.6	−130.9
Vertical	3428.5	3312.7

CE: location based on main sail tag

Coordinates positive to stern, to top (mm)

The computed results for the sail system were compared with existing experimental data [6]. It was found that the jib angle is a key parameter, since the flow interaction between the jib and the main sail depends on it. Furthermore, the jib sail generates more lift force than the main sail. It is also found that the CE estimated from the geometric center was quite different from the CE calculated from the computed pressure distribution.

Acknowledgments The present study was supported by the Ministry of Knowledge Economy (MKE) through the Regional Innovation Center and by the Ministry of Education, Science and Technology (MEST) through NRF Grant No. 2009-0087863. The fourth author was separately supported by MEST through a World Class University project (R32-10161) and the Multi-phenomena CFD Research Center (NRF Grant No. 2009-0083510).

References

1. Larsson L, Eliasson RE (2000) Principles of yacht design, 2nd edn. International Marine, Camden
2. Rosen BS, Laiosa JP, Davis WH Jr. (2000) CFD design studies for America's Cup 2000 (AIAA Paper 2000-4339). In: Proc 18th AIAA Applied Aerodynamics Conf and Exhibit, Denver, CO, 14–17 August 2000
3. Akimoto H, Miyata H (2002) Finite-volume simulation method to predict the performance of a sailing boat. J Mar Sci Technol 17(1):31–42
4. Jasak H (2009) OpenFOAM: open source CFD in research and industry. Int J Nav Archit Ocean Eng 1(2):89–94
5. DeBord F Jr, Reichel J, Rosen B, Fassardi C (2002) Design optimization for the International America's Cup Class. In: Trans SNAME Annual Meeting, Boston, MA, 25–28 September 2002
6. Yoo JH, Kim HT (2006) Computational and experimental study on performance of sails of a yacht. Ocean Eng 33(10):1322–1342
7. Yoo JH, Van SH, Ahn HS, Kim J, Kim SH (2005) Development of 30 feet sailing yacht and performance predictions. J Soc Nav Archit Korea 42(1):34–42 (in Korean)
8. Yoo JH, Ahn HS (2005) Experimental study on the hydrodynamic forces of 30 feet sailing yacht. J Soc Nav Archit Korea 42(3):233–240 (in Korean)
9. Yang J, Rhee SH, Kim H (2009) Propulsive performance of a tanker full form in damaged conditions. Ocean Eng 36(2):133–144